Modular Type III Porous Liquids based on Porous Organic Cage Microparticles

Aiting Kai,[a] Benjamin D. Egleston,[a] Marc A. Little,[a] Rob Clowes,[a] Michael E. Briggs,[a] Andrew I Cooper [a*] and Rebecca L. Greenaway[a,b*]

[a] Department of Chemistry and Materials Innovation Factory, University of Liverpool, 51 Oxford Street, Liverpool, L7 3NY, UK

[b] Department of Chemistry, Molecular Sciences Research Hub, Imperial College London, White City Campus, 82 Wood Lane, W12 0BZ, UK.

Email: aicooper@liverpool.ac.uk; r.greenaway@imperial.ac.uk

The dispersion of particulate porous solids in size-excluded liquids has emerged as a method to create Type III porous liquids, mostly using insoluble microporous materials such as metal-organic frameworks (MOFs) and zeolites. Here, we present the first examples of Type III porous liquids based on porous organic cages (POCs). By exploiting the solution processability of the POCs, racemic and quasiracemic cage microparticles were formed by chiral recognition. Dispersion of these porous microparticles in a range of size-excluded liquids, including oils and ionic liquids, formed stable POC-based Type III porous liquids. The flexible pairing between the solid POC particles and a carrier liquid allows the formation of a range of compositions, pore sizes, and other physicochemical properties to suit different applications and operating conditions. For example, we show that it is possible to produce porous liquids with relatively low viscosities (7-14 mpa·s) or high thermal stability (325 °C). A 12.5 wt. % Type III porous liquid comprising racemic POC microparticles and an ionic liquid, [BPy][NTf$_2$], shows a CO_2 working capacity (104.30 μmol/g$_L$) that is significantly higher than the neat ionic liquid (37.27 μmol/g$_L$) between 25 °C and 100 °C. This liquid is colloidally stable and can be recycled at least 10 times without loss of CO_2 capacity.

Introduction

Porous liquids are a novel kind of porous material that are distinguished by their ability to flow. These materials have seen considerable progress since the concept was first introduced in 2007 by O'Reilly *et al*.[1] Three types of porous liquids were initially proposed (Types I, II and II; Figure 1a) and after more than a decade, examples of each type have now been reported.[2] Type I porous liquids are neat liquid substances with shape-persistent molecular porosity; Type II porous liquids are solutions of natively porous molecules dissolved in a 'non-porous' solvent, where the pores remain unoccupied because the solvent molecules are size excluded; Type III porous liquids are multiphase fluids, typically porous solids particles dispersed in size-excluded liquids. Type III porous liquids are typically simpler to prepare than the other two types, and this approach might prove to be more generalizable in the future. For Type I porous liquids, it is necessary to devise strategies for lowering the melting points of shape-persistent porous molecules, such as cages and macrocycles, and the viscosity of such liquids may also be limiting. Type II porous liquids are somewhat easier to access, though this requires strategies for increasing the solubility of the pore carriers in the size-excluded solvents, and again viscosity may be an issue at high concentrations of the pore carrier. By contrast, the formation of Type III porous liquids can be approached in a modular way, and it is feasible to screen a wide range of porous materials and bulky liquids to find suitable combinations.[3] This modular approach might prove more industrially applicable, not least because one can draw on a large range of existing materials as building blocks, some of which have already been scaled up.[4] So far, Type III porous liquids have mostly been constructed from metal-organic frameworks (MOFs) and zeolites. For example, ZIF-8 was found to be dispersible in several large hindered ionic liquids,[5–7] or in polymeric glycols,[8] while Cahir *et al.* reported the formation of a range of Type III porous liquids using various microporous solids, including MOFs and zeolites, in non-ionic oils.[3] Until now, Type III porous liquids have been built from extended porous materials that are insoluble in common liquids.

Porous organic cages (POCs) are a type of molecular organic material that contains shape-persistent internal voids in the molecules that are accessible through windows.[9–11] Imine-derived POCs can be synthesized in solution through a reversible condensation reaction, and many derivatives can be produced based on the selection of different synthetic precursors: a representative scheme for preparing the POCs used in this study is shown in Figure 1b. The window sizes and chemical environment of POCs can be tuned by introducing different functional groups into the precursors.[12] POCs can also have good solubility in organic solvents, and are thus a candidate for preparing Type II porous liquids.[13–15] There have also been attempts to decorate cages with long alkyl chain functionality to lower the melting points in the preparation of Type I porous liquids.[16,17] Some of the properties of POCs can be retained when transferred into the liquid state, such as size-selective guest uptake,[18] while others, such as chiral recognition,[14] are lost. One potential way to retain the solid-state properties of POCs is to form Type III porous liquids, rather than Type I or Type II systems.
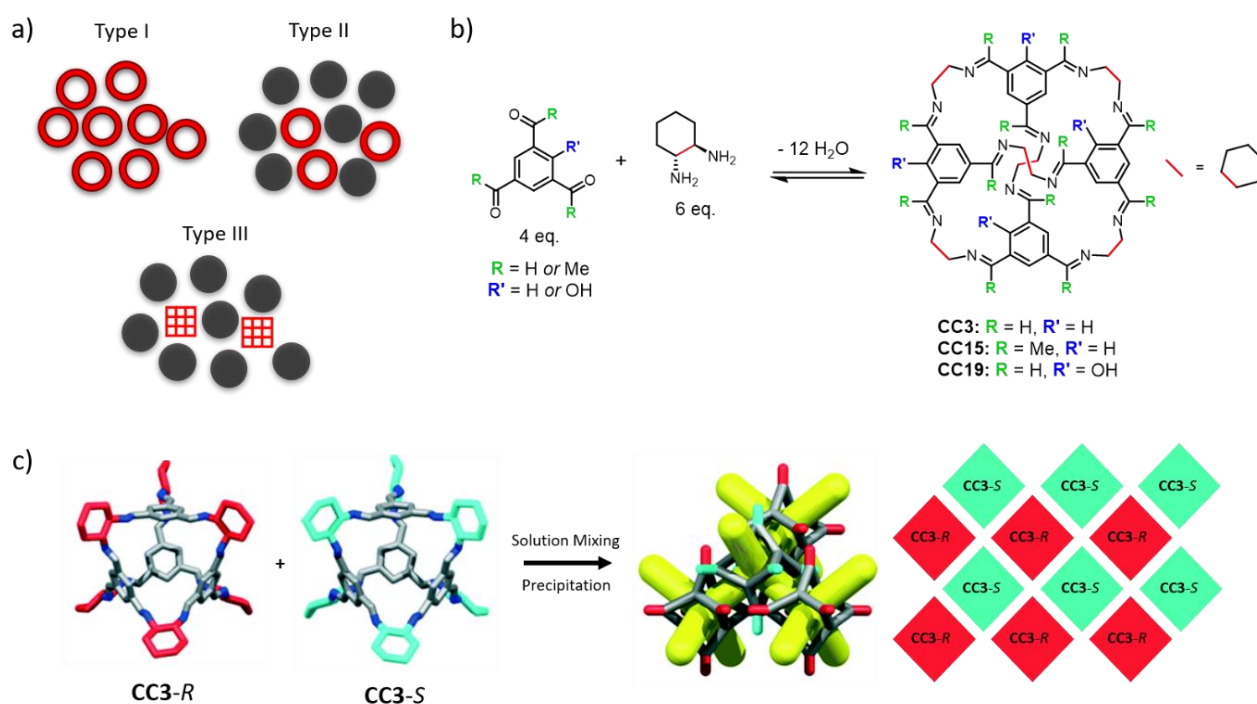
Figure 1: (a) Scheme showing the three classifications of porous liquids: Type I, Type II, and Type III; (b) General reaction scheme for the synthesis of **CC3**, **CC15**, and **CC19**, which are the POCs used to form microparticles in this study. Two cage enantiomers can be formed for each species; for example **CC3**-*R* and **CC3**-*S* can be formed by using the different enantiomers of *trans*-1,2-cyclohexyldiamine (CHDA), (*R,R*)-CHDA, and (*S,S*)-CHDA; (c) POCs such as **CC3** can pack together window-to-window to form a 3D diamondoid pore network in the solid state by chiral recognition between the two cage enantiomers, which can be exploited to form POC microparticles for processing into Type III porous liquids.[19]

As a multiphase system, the colloidal stability of Type III porous liquids is an important consideration. For example, Dai *et al.* used hydrogen bonding between H-ZSM-5 zeolites and bulky phosphonium ionic liquids to construct a colloidally stable Type III system,[20] whereas Li *et al.* and Liu *et al.* used surface functionalisation to coat particles of UiO-66 or Silicalite-1 respectively with solvent-similar polymeric groups to stabilise these as Type III porous liquids.[21,22] More recently, the surface functionalisation method was also used to form a stabilised ZIF-67 dispersion, which can be used directly as a Type III porous liquid or conveniently processed further to form mixed matrix membranes with excellent selectivity between propane and propylene.[23] While a 3D imine-linked covalent organic framework (COF) was functionalised with ionic liquid functionality on its outer shell, forming COF colloids that were extremely stable towards flocculation (> one year) in an ionic liquid.[24] Alternatively, in ZIF-8 based Type III porous liquids, a rapid synthetic method can be employed to produce nanocrystalline particles that allow for stable emulsions when the solid ZIF-8 is dispersed.[25]

POC nano- and micro-particles can also be easily fabricated from solution by exploiting the chiral recognition between two prefabricated homochiral precursor cages, producing co-crystals in a modular way without the

3

use of any surfactants or templating agents.[19,26] These can either be prepared from enantiomeric variants of the same cage species to form a racemate (Figure 1c), or formed from isostructural cage derivatives of opposite chirality to produce quasiracemic co-crystals.[27–29] By using two chemically different cages to form quasiracemic co-crystals, it is possible to tune the properties of the pore carrier, such as the pore size or the chemical environment in the pores – for example, to produce materials with superior properties for quantum sieving of hydrogen isotopes.[30] Furthermore, upon co-crystallisation, the solubility of these racemic and quasiracemic cage materials is often greatly reduced compared to the solution-processable enantiopure cage precursors, thus making them good candidates for preparing Type III porous liquids.

Here, we report the first use of POC assembled microparticles to form stable Type III porous liquids. Different compositions of cage microparticles (**CC3**-*R/***CC3**-*S*, **CC3**-*R/***CC15**-*S*, and **CC3**-*R/***CC19**-*S*) were dispersed in a selection of size-excluded liquids including a range of oils and ionic liquids, and their gas uptakes were investigated. Overall, a versatile Type III porous liquid platform can be built using different POCs in neat liquids, without the need for any surfactants or post-synthetic modification, with physical properties that can be tailored according to the application.

Results and Discussion

Synthesis and Characterisation of POC Microparticles

First, the formation of three different POC microparticles was investigated: racemic **CC3**-*R/***CC3**-*S*, quasiracemic **CC3**-*R/***CC15**-*S*, and quasiracemic **CC3**-*R/***CC19**-*S* (Figure 2a). The synthesis of **CC3**-*R/***CC3**-*S* microparticles by chiral recognition was reported previously, where homochiral solutions of **CC3**-*R* and **CC3**-*S* were mixed and uniformly fine microparticles were formed.[19] Using a slight modification of that method, multiple large scale batches of **CC3**-*R/***CC3**-*S* microparticles were formed by rapidly mixing dilute solutions of both **CC3**-*R* and **CC3**-*S* in dichloromethane at room temperature with overhead stirring (Table 1, entries 1-5). Rapid precipitation of the POC microparticles was observed upon mixing, which were isolated by filtration. An additional batch of **CC3**-*R/***CC3**-*S* was formed using a carefully controlled addition rate for comparison (Table 1, entry 6). We also investigated the formation of **CC3**-*R/***CC15**-*S*, and **CC3**-*R/***CC19**-*S*, with crystallisation of **CC3**-*R/***CC19**-*S* occurring rapidly using the same method as with **CC3**-*R/***CC3**-*S* (Table 1, entry 8). However, for **CC3**-*R/***CC15**-*S*, rapid precipitation did not occur under these conditions; this is thought to be due to the methyl groups in **CC15**, which reduces the favourable interaction between the cage windows that promotes rapid co-crystallisation. Slater *et al.* generated co-crystals of **CC3**-*R/***CC15**-*S* from dichloromethane using five-fold more concentrated solutions of the two cages, although small particle sizes were not targeted in that study.[12] We found that microcrystalline particles of **CC3**-*R/***CC15**-*S* could be

4

prepared at the same dilute concentration by changing the solvent to a 1:1 mixture of dichloromethane:methanol (Table 1, entry 7).
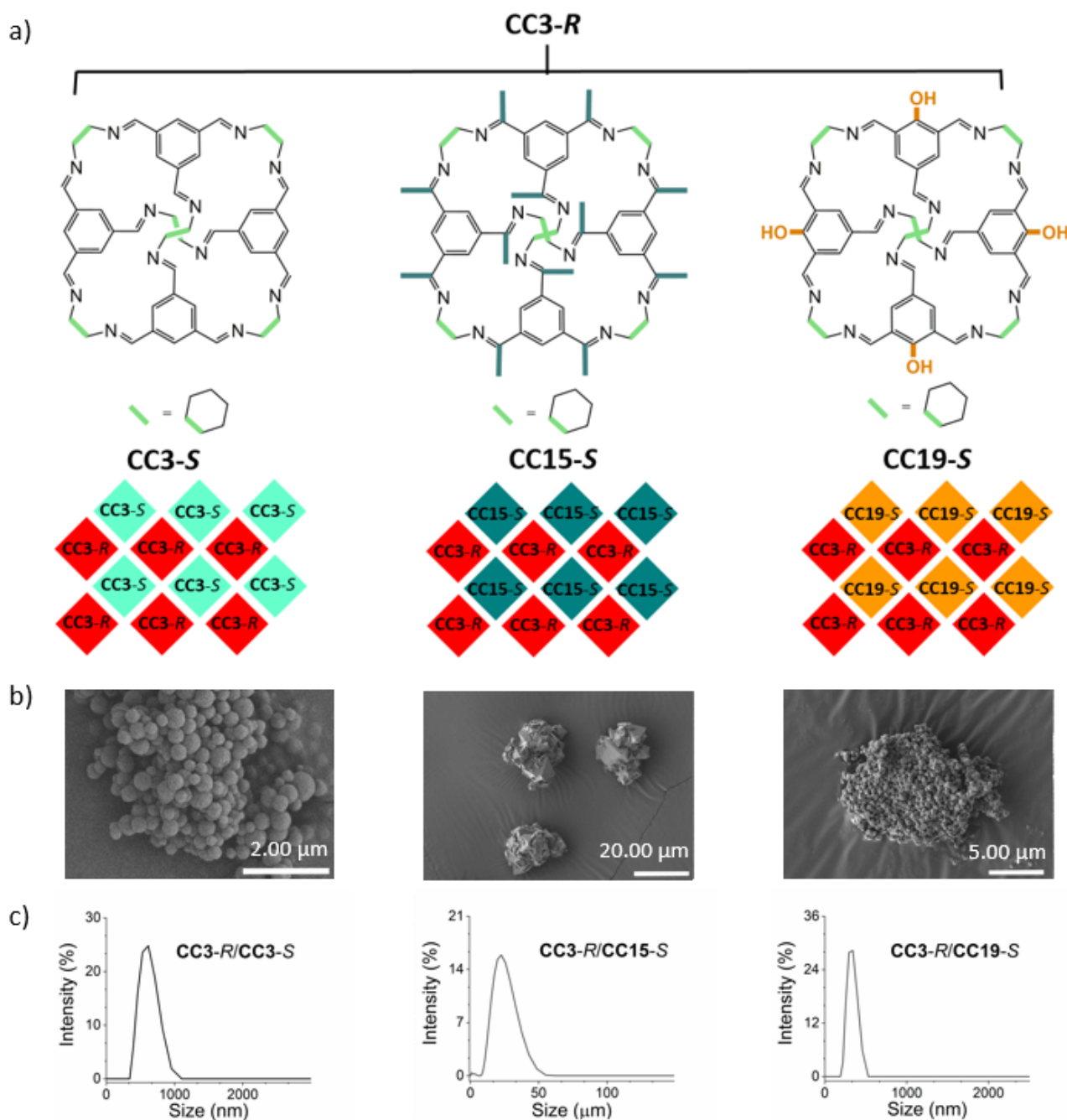

Figure 2: (a) Scheme for POC microparticle formation by combining **CC3**-*R* and with either **CC3**-*S*, **CC15**-*S*, or **CC19**-*S*; (b) Scanning electron micrographs for **CC3**-*R*/**CC3**-*S*, **CC3**-*R*/**CC15**-*S*, and **CC3**-*R*/**CC19**-*S* microparticles; (c) Particle size distributions of **CC3**-*R*/**CC3**-*S* (by DLS in dichloromethane), **CC3**-*R*/**CC15**-*S* (by SLS in EtOH), and **CC3**-*R*/**CC19**-*S* (DLS in dichloromethane).

Analysis of these co-crystals confirmed they were the desired microparticles (Table 1), as determined by dynamic light scattering (DLS) measurements and scanning electron microscopy (SEM), with diameters for **CC3**-*R/***CC3**-*S* and **CC3**-*R*/**CC19**-*S* ranging from ~200 nm to 1.5 μm (Figure 2b-2c). The **CC3**-*R*/**CC15**-*S* particle size could not be measured using the solvents that we deployed for DLS because sedimentation occurred in MeOH, while the co-crystal dissolved in dichloromethane. However, by using static light scattering (SLS) measurements, these particles were found to be significantly larger (17 μm). This reflects the slower precipitation of these particles, which gives them the chance to increase in size. SEM also gave an indication of the particle morphology; when **CC3**-*R/***CC3**-*S* was isolated after rapid mixing, the microparticles were spherical, whereas on slow addition, octahedral particles were formed (Figure S4). For **CC3**-*R*/**CC19**-*S*, SEM images also confirmed an octahedral morphology when using the rapid addition technique, whereas for **CC3**-*R*/**CC15**-*S,* larger blocks of crystals with blended octahedral morphology were apparent, which corresponded to the larger particles observed by SLS (Figure S8). Analysis by powder x-ray diffraction (PXRD) showed results that were consistent with previous studies; the co-crystals had powder patterns that were similar to **CC3α**, but with peak shifts that reflected smaller unit cell sizes (Figure S3). This indicates that all co-crystals adopt a window-to-window arrangement, with tighter packing due to the use of opposite cage enantiomers.

Table 1: Summary of the microparticle composition, particle sizes, and particle morphology.

Entry	Composition	DLS Size / nm	SEM Size Range / nm	Morphology
1	**CC3**-*R/***CC3**-*S*	540	200–700	Spherical
2	**CC3**-*R/***CC3**-*S*	600	300–800	Spherical
3	**CC3**-*R/***CC3**-*S*	1200	300–1000	Spherical
4	**CC3**-*R/***CC3**-*S*	720	300–1000	Spherical
5	**CC3**-*R/***CC3**-*S*	630	200–800	Spherical
6	**CC3**-*R/***CC3**-*S*	940	200–1500	Octahedral
7	**CC3**-*R*/**CC15**-*S*	17,000[a]	8000–31000	Octahedral
8	**CC3**-*R*/**CC19**-*S*	300	200–800	Octahedral

[a]Particle size determined with static light scattering (SLS) measurements.

Screening for Type III Porous Liquids using POC Microparticles

We first carried out a screen for suitable size-excluded liquids to construct Type III porous liquids using the **CC3**-*R/***CC3**-*S* microparticles (Table 1, entries 3 and 5). A range of liquids was selected, including different oils and ionic liquids (Figure 3a), some of which were reported previously to be size-excluded for MOFs and

zeolites, such as silicone oil, pyridinium bis(trifluoromethanesulfonyl)imide ([BPy][NTf$_2$]), and trihexyltetradecylphosphonium bis(trifluoromethanesulfonyl)imide ([P$_{66614}$][NTf$_2$]).[3,6,7] A 12.5 wt. % dispersion of **CC3**-*R/***CC3**-*S* microparticles was prepared in these liquids by mixing and sonication. For oils that were more viscous, such as Halocarbon 27® and Fomblin Y®, 5 wt. % loadings were prepared to obtain a flowable dispersion. These dispersions were then screened for porosity to allow comparison of the gas uptakes with the neat, unadulterated liquids. Previously, analytical techniques such as IR and NMR spectroscopy, or gas displacement measurements, were used to probe the gas solubility in POC-derived Type II porous liquids.[13–15,18] Here, the use of bulky liquids with high boiling points and low vapour pressures allowed us to study the gas solubility using more standard sorption measurements that are used for porous solids. Specifically, the use of a Quantachrome Nova instrument, benchmarked to known uptakes in liquids and with stirring to ensure that the liquids reached saturation uptake, allowed different gases to be screened and adsorption isotherms to be obtained (see ESI, Section 1, for more information).

Comparison of the CO_2 uptakes at 1 bar in the neat liquids and the corresponding **CC3**-*R/***CC3**-*S* dispersions (Table S3, Figure S9a–S9k) indicated that most of the dispersions showed a marked improvement in CO_2 solubility over the neat liquid (Figure 3b). An exception was a 12.5 wt. % dispersion in Genosorb 1753®, where the neat liquid absorbed more CO_2 than the dispersion, suggesting perhaps that the liquid molecules can occupy the pores in the **CC3**-*R/***CC3**-*S* microparticles. It should also be noted that Genosorb liquids are designed specifically to absorb CO_2, and hence have a relatively high native CO_2 solubility in any case. The most marked increases in CO_2 solubility were found with silicone oil (5 cSt), silicone oil AR 20, and [BPy][NTf$_2$]. Comparison of the measured uptakes with theoretical maximum uptakes for each dispersion, calculated by taking into account the proportions of the cage solid and the liquid (Table S4), found that 59–66% of the overall theoretical maximum porosity was obtained for these three liquids. The 5 wt. % **CC3**-*R/***CC3**-*S* dispersions in Halocarbon 27® and Fomblin Y® also displayed 57–60% of the maximum theoretical porosity, but higher solid loadings led to highly viscous systems that did not flow. The remaining dispersions ranged from 25-46% of the maximum theoretical porosity. The observed reductions in uptake are likely due to the loss of some extrinsic porosity when **CC3**-*R/***CC3**-*S* is dispersed, and the potential viscosities of each dispersion affecting the diffusion of gas through the system, but the increased uptakes indicated the successful formation of Type III porous liquids. Additionally, all of these dispersions were visually stable after standing at room temperature for at least 24 hours.

In order to gain a further understanding of these systems, the **CC3**-*R/***CC3**-*S* dispersions in both silicone oil and [BPy][NTf$_2$] were selected for further studies. These 12.5 wt. % dispersions illustrated the greatest enhancement in CO_2 uptake over the neat liquids, for example, in silicone oil the dispersion illustrated a ~ 2-fold increase in capacity (198 ± 3.8 µmol/g$_L$ vs. 84.8 ± 2.4 µmol/g$_L$ for pure silicone oil). A similar increase was also observed for the dispersion in [BPy][NTf$_2$] (172.1 ± 3.6 µmol/g$_L$ vs. 78.3 ± 4.5 µmol/g$_L$ for pure

[BPy][NTf$_2$]). These liquids also had the lowest viscosities in each class out of the oils and ionic liquids, allowing higher weight loadings to be studied.
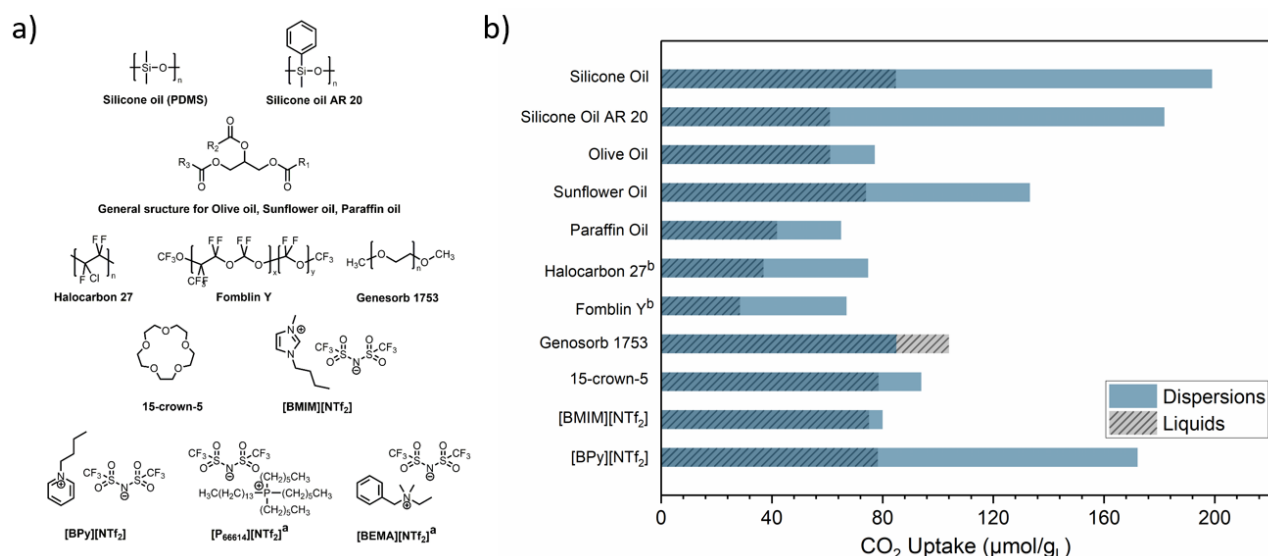

Figure 3: (a) Bulky liquids screened in this study for the formation of Type III porous liquids with **CC3**-*R*/**CC3**-*S* POC microparticles; (b) Comparison of the CO_2 uptakes for the neat bulky liquids and corresponding 12.5 wt. % dispersions of **CC3**-*R*/**CC3**-*S*. [a] Ionic liquids screened with homochiral cage **CC3** instead of **CC3**-*R*/**CC3**-*S* POC microparticles to determine if homochiral POCs can be used as a rapid indicator of size-exclusivity and porosity; [b] A 5 wt. % dispersion was studied to reduce viscosity.

Comparison of Type III POC Microparticle Porous Liquids with Control Liquids

In our preliminary screen, **CC3**-*R*/**CC3**-*S* dispersions led to similar gas uptake improvements in different liquids (*e.g.*, silicone oil vs. [BPy][NTf$_2$]; Figure 4a), indicating that the enhanced gas uptake was related to the **CC3**-*R*/**CC3**-*S* microparticles introducing extra pore volume into the liquid. To further confirm that the observed improvement in CO_2 uptake was due to the internal pore space of the **CC3**-*R*/**CC3**-*S* microparticles, rather than, say, surface adsorption on the microparticles, a control molecule that mimics a fragment of the **CC3** cage was synthesized (Figure 4b inset).[14] This non-porous control molecule does not dissolve in silicone oil or [BPy][NTf$_2$], and thus can also be dispersed, allowing us to evaluate the effect of surface adsorption on the particles in the system. CO_2 isotherms were measured on dispersions of the control molecule in both silicone oil and [BPy][NTf$_2$] for direct comparison with the **CC3**-*R*/**CC3**-*S* dispersions. No improvement in CO_2 uptake was observed in either system, confirming that surface adsorption does not contribute measurably to the observed improvements in gas uptake (Figure 4b). Additionally, in contrast to the microparticle dispersions in the same liquids, dispersions of the control molecule were not stable, with sedimentation rapidly occurring (< 1 hour) on standing.

8

Dispersions of homochiral cage **CC3**-*R* in silicone oil, and **CC3**-*S* in [BPy][NTf$_2$], were also investigated for their gas solubility – while similar gas uptakes were obtained compared to the **CC3**-*R/***CC3**-*S* microparticle systems (Figure 4c), the homochiral dispersions were not as colloidally stable, with sedimentation occurring when stirring was not maintained at room temperature. However, this further confirms that these liquids are size-excluded from **CC3**, and that homochiral cages could be used to rapidly determine whether new liquids are size-excluded prior to forming POC microparticles with controlled particle sizes and narrow distributions. For example, measurement of the CO$_2$ uptake in dispersions of **CC3**-*S* in [P$_{66614}$][NTf$_2$] and benzyl(ethyl)dimethylammonium bis(trifluoromethanesulfonyl)imide ([BEMA][NTf$_2$]) demonstrated that these two ionic liquids were size-excluded (Figure 3a, Figure S9l-S9m).

Finally, different batches of **CC3**-*R/***CC3**-*S* microparticles were investigated to evaluate the effects of particle size and surface morphology on the gas uptake. Dispersions of **CC3**-*R/***CC3**-*S* with particle sizes of 600 nm and 720 nm (Table 1, entry 2 and 4) show similar CO$_2$ solubility compared to dispersions with particle sizes of 1200 nm and 630 nm (Table 1, entry 3 and 5), in silicone oil and [BPy][NTf$_2$] respectively (Figure 4a). When **CC3**-*R/***CC3**-*S* with an octahedral morphology (Table 1, entry 6) was used, its dispersion presented similar gas uptakes to spherical **CC3**-*R/***CC3**-*S* microparticles (Figure 4d). Overall, this shows that the particle size and morphology has little if any effect on the gas uptake of the dispersions, but that controlling the particle size is important for ensuring good, long-term dispersion stability.
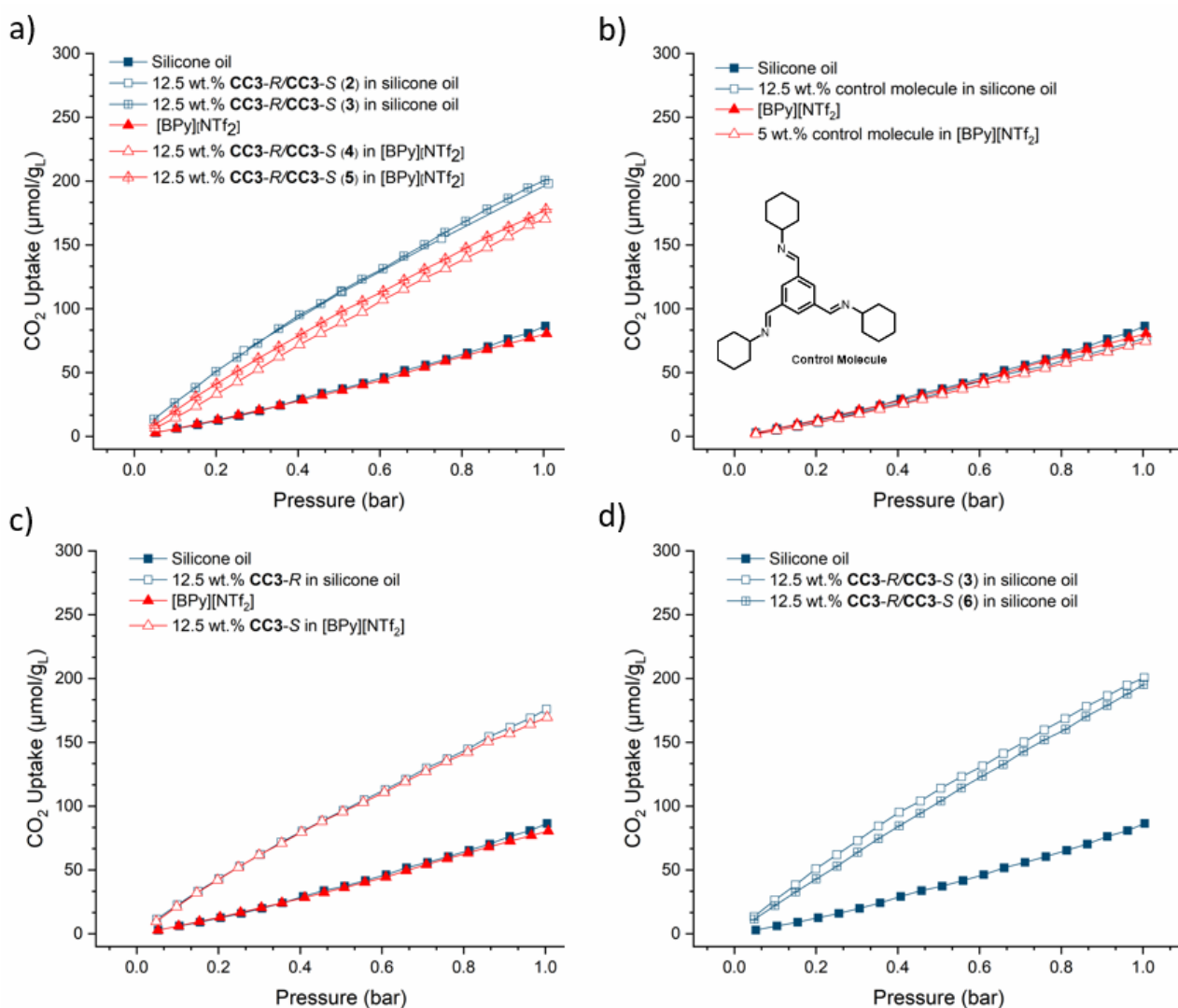
Figure 4: (a) CO_2 adsorption isotherms of 12.5 wt. % dispersions of **CC3-*R*/CC3-*S*** with varying particle sizes in silicone oil and [BPy][NTf$_2$]; (b) CO_2 adsorption isotherms of non-porous control molecule dispersions in silicone oil and [BPy][NTf$_2$], with inset showing the structure of the control molecule; (c) CO_2 adsorption isotherms of homochiral cage **CC3** dispersions in silicone oil and [BPy][NTf$_2$]; (d) CO_2 adsorption isotherms of 12.5 wt. % dispersions of **CC3-*R*/CC3-*S*** with different particle morphologies in silicone oil. The numbers in brackets indicate the batch of microparticles used from Table 1.

Gas Uptake, properties and stability of Type III CC3-*R*/CC3-*S* Microparticle Porous Liquids

To be put into practical use, porous liquids should offer favourable characteristics, such as being recyclable and thermally stable. We selected two systems from the initial screen—**CC3-*R*/CC3-*S*** in silicone oil and in [BPy][NTf$_2$]—to more fully study their physicochemical properties. Different loadings of **CC3-*R*/CC3-*S*** microparticles (5, 12.5, and 20 wt. %) were prepared in both liquids to evaluate the effect of microparticle concentration on both the gas uptake and the dispersion viscosity.

The viscosity of the dispersions in [BPy][NTf$_2$] was higher than those in silicone oil (Table 2), which is due to the general viscous nature of ionic liquids.[28] However pure [BPy][NTf$_2$] has a viscosity of 67.34 mpa·s, which

is substantially lower than the viscosity of other size-excluded ionic liquids; for example, $[P_{66614}][NTf_2]$ and $[BEMA][NTf_2]$ have viscosities of 395.7 mpa·s and 496.6 mpa·s, respectively. Viscosity studies on the 5, 12.5, and 20 wt. % dispersions of **CC3**-*R*/**CC3**-*S* microparticles in $[BPy][NTf_2]$ and in silicone oil showed that the viscosity of the dispersions increased with increasing particle concentration (Table 2). However, while the ionic liquid dispersions had relatively higher viscosities, which could slow down gas adsorption kinetics, the saturated gas solubilities appeared to be unaffected: both CO_2 and CH_4 uptakes increased linearly with increasing **CC3**-*R*/**CC3**-*S* content from 0 to 20 wt. % for both the $[BPy][NTf_2]$ and silicone oil based dispersions (Figure 5a, Figure S10-S13). At 20 wt. % the uptakes were fairly comparable across both systems, although the overall uptakes for both gases were slightly higher in the silicone oil dispersion (CO_2: 280 µmol/g_L vs 210 µmol/g_L; CH_4: 121 µmol/g_L vs 103 µmol/g_L). Dispersions of **CC3**-*R*/**CC3**-*S* in silicone oil were also investigated up to 50 wt. %, with a linear trend for CO_2 adsorption again being observed up to 635 µmol/g_L at 50 wt. % (Figure 5b and S14).

The dispersion in $[BPy][NTf_2]$ demonstrates good thermal stability according to thermal gravimetric analysis (TGA, Figure 5c), with no significant mass loss observed until 325 °C. However, the low viscosity silicone oil used in these studies (PDMS, 5 mpa·s) has a significantly higher vapour pressure (<700 Pa at 298.15 K)[31] compared to $[BPy][NTf_2]$ (0.0519 Pa at 498.07 K),[32] and the corresponding porous liquid therefore demonstrates a much lower thermal stability, with mass loss occurring from 60 °C based on TGA analysis (Figure S15). This does not cause significant problems for the gas sorption measurements carried out here, with the degassing and uptake measurements performed immediately after sample preparation at ambient temperature, but this increased volatility might account for the slightly elevated CO_2 adsorption isotherm of a 12.5 wt. % silicone oil dispersion after ~ 1 month compared to after 1 day, possibly due to slow evaporation of the liquid over time making the porous liquid more concentrated, while the gas uptake remained nearly unchanged for the aged $[BPy][NTf_2]$ sample (Figure 5d).

For these two systems, the viscosity and thermal stability are essentially trade-offs; ideally, one would like a high thermal stability liquid with low viscosity to allow the broadest range of potential applications. We note that the thermal stability limit is imposed by the liquid, rather than the POC.

Table 2: Summary of viscosity measurements on the liquids and different concentration dispersions investigated.

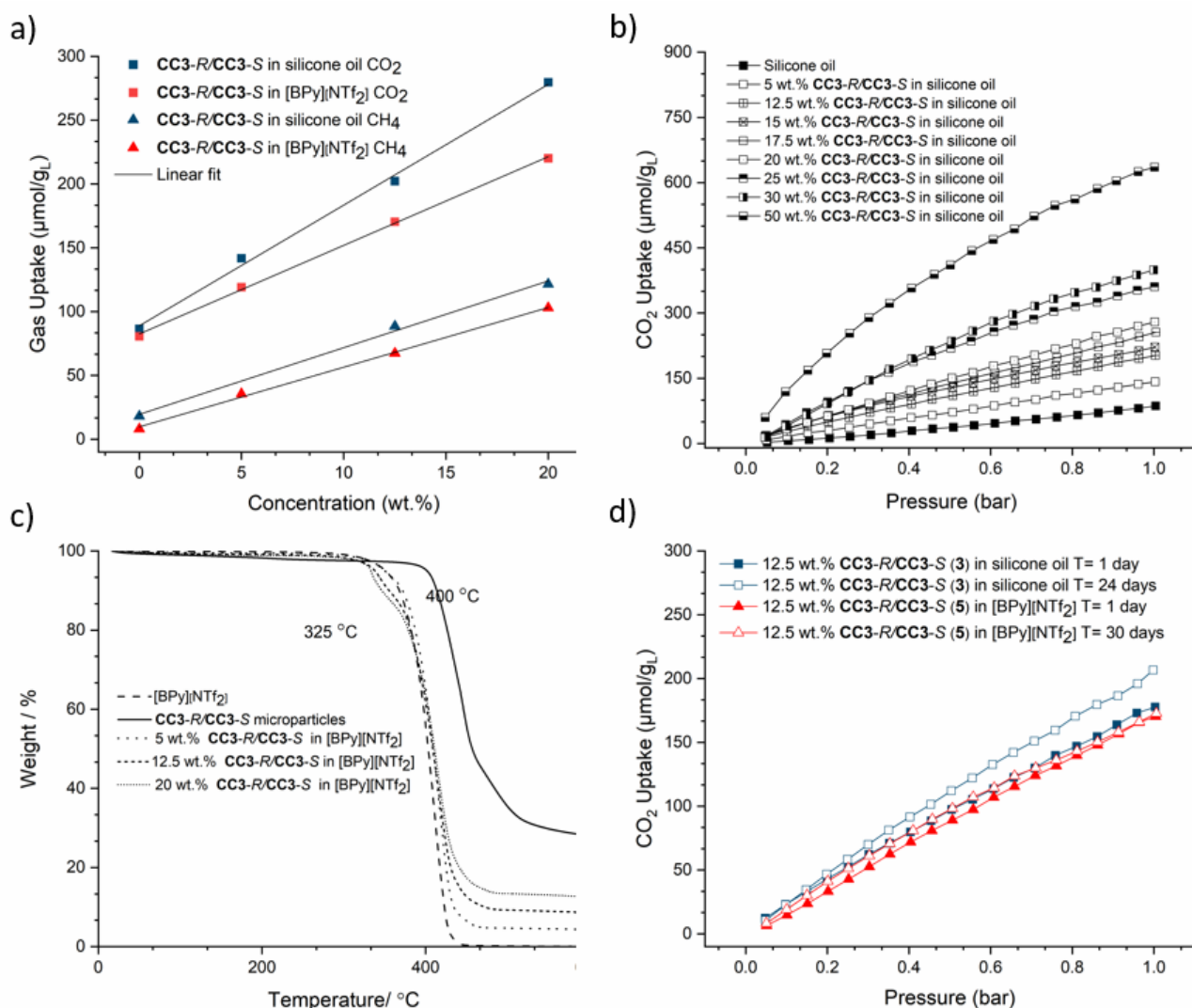| Liquids	Viscosity (mpa·s)			
	0 wt. % Dispersion	5 wt. % Dispersion	12.5 wt. % Dispersion	20 wt. % Dispersion
Silicone Oil	5.01 ± 0.01	7.41 ± 0.09	13.22 ± 0.55	19.09 ± 0.60
[BPy][NTf$_2$]	67.34 ± 0.06	86.18 ± 0.16	142.2 ± 0.14	303.5 ± 0.29

Figure 5: (a) Measured gas uptakes for a range of **CC3**-*R/***CC3**-*S* dispersions at different concentrations (1 bar, 298-300 K); (b) CO_2 adsorption isotherms of silicone oil and the corresponding 5, 12.5, 15, 17.5, 20, 30 and 50 wt. % dispersions of **CC3**-*R/***CC3**-*S* microparticles; (c) TGA of [BPy][NTf$_2$] and 5, 12.5 and 20 wt. % **CC3**-*R/***CC3**-*S* dispersions in [BPy][NTf$_2$]; (d) CO_2 adsorption study of aged dispersion samples.

While there is a trade-off between the viscosity and thermal stability for dispersions in silicone oil (PDMS, 5 mpa·s) vs [BPy][NTf$_2$], the other physical properties for these two porous liquids are broadly similar. Both systems retain their porosity over time (Figure 5d). To evaluate the recyclability of these liquids as gas sorbents, the CO$_2$ uptake was measured over 10 cycles in a 12.5 wt. % dispersion of **CC3**-*R*/**CC3**-*S* in [BPy][NTf$_2$] (Figure 6a and Figure S16), with re-activation by vacuum degassing for 100 minutes carried out between measurements. The CO$_2$ uptakes were reproducible, with no loss in uptake apparent over repeated cycles (average CO$_2$ uptake over 10 cycles: 174.3 ± 4.6 µmol/g). Due to the slight volatility of the silicone oil, the corresponding 12.5 wt. % dispersion was only cycled twice, but again, the CO$_2$ solubility was completely reproducible over two cycles (Figure S17).

The cage microparticle and phase stability of both dispersions was also investigated in more detail. The crystallinity of the **CC3**-*R*/**CC3**-*S* microparticles was retained upon formation of dispersions in silicone oil and [BPy][NTf$_2$] (Figure S18–S19), and no phase change was observed post-sorption (Figure S20). Both the silicone oil and [BPy][NTf$_2$] dispersions of **CC3**-*R*/**CC3**-*S* microparticles appeared to be visually stable over extended periods. To quantify the dispersion stability, a LUMiSizer® was used to accelerate the creaming or sedimentation process for 12.5 wt. % dispersions of **CC3**-*R*/**CC3**-*S* (particle size: 500–700 nm) in both silicone oil and [BPy][NTf$_2$].[33] According to Stoke's law, particle size plays an important role in determining the ratio of gravitational to Brownian forces applied to the particles in a dispersion, and hence reducing the particle size can help to control the sedimentation velocity and thus stabilise multiphase systems.[34] At a relative centrifugal force of 532 × g, the **CC3**-*R*/**CC3**-*S* microparticles separate by creaming to the surface of the silicone oil at a sedimentation velocity of 0.24 mm/day, indicating that the dispersion is stable (Table S7, Figure S21). The [BPy][NTf$_2$] system also showed creaming but had a reduced sedimentation velocity of 0.04 mm/day, indicating that this dispersion has improved stability over the one in silicone oil (Table S7, Figure S23). This could be due to the increased viscosity of the ionic liquid, or potentially because the cation and anion of [BPy][NTf$_2$] provide electrostatic stabilization for the POC particles.[35]

Finally, the increased thermal stability of [BPy][NTf$_2$] allowed for further adsorption studies to be carried out at higher temperatures to investigate the potential of a temperature-swing process for gas uptake and release. The CO$_2$ uptakes of neat [BPy][NTf$_2$] and its corresponding 12.5 wt. % **CC3**-*R*/**CC3**-*S* dispersion were measured at a range of temperatures: 25, 40, 60, 80 and 100 °C (Figure 6b, and Figures S24-S25). Both systems showed measurable uptakes, even when the temperature was increased to 100 °C, which might arise from the strong interaction of CO$_2$ with the ionic liquid, but the working absorption capacity of **CC3**-*R*/**CC3**-*S* in [BPy][NTf$_2$] was significantly larger than for neat [BPy][NTf$_2$] (104.30 µmol/g$_L$ vs 37.27 µmol/g$_L$ between 25 °C and 100 °C).
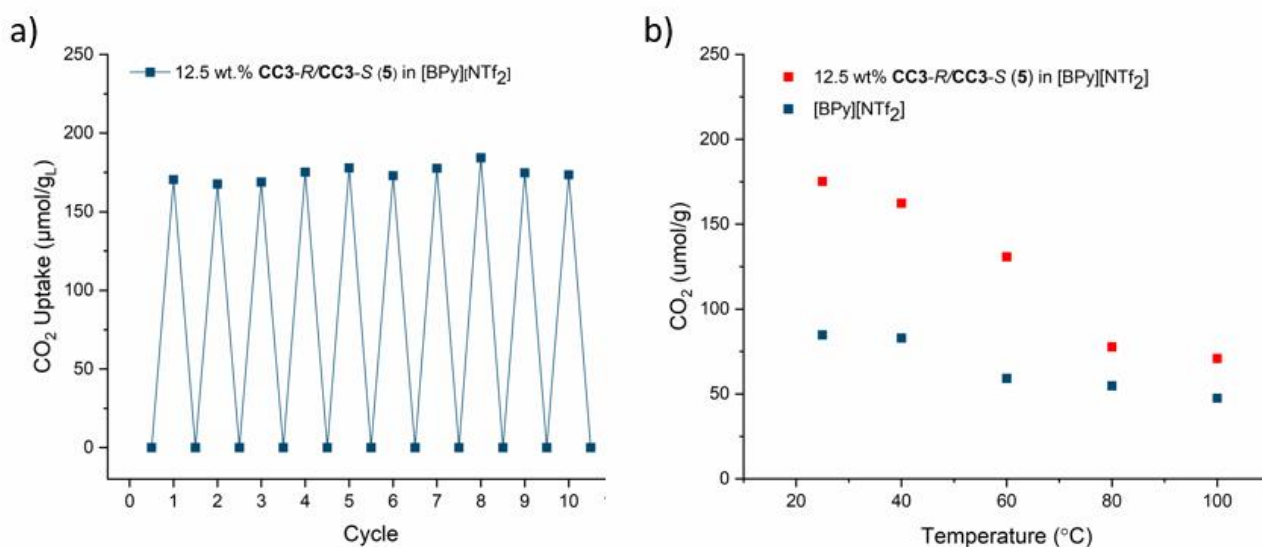
Figure 6: (a) Recycling study for CO_2 uptake (1 bar, 298-300 K) in a 12.5 wt. % dispersion of **CC3**-*R/***CC3**-*S* in [BPy][NTf$_2$]; (b) CO_2 solubilities in [BPy][NTf$_2$] and the corresponding 12.5 wt. % **CC3**-*R/***CC3**-*S* dispersion at 25, 40, 60, 80, and 100 °C. The Type III porous liquid has a higher working capacity (104.30 $\mu mol/g_L$) than the neat ionic liquid (37.27 $\mu mol/g_L$) between 25 °C and 100 °C.

Modification of porosity in Type III PLs by the modular assembly of two POCs into microparticles

Controlling POC pore structure to influence the gas uptake has been studied widely in the solid state, for example by introducing bulky groups to decrease the window or cavity sizes, as applied in Xe or hydrogen isotope separation.[12,30] Likewise, specific functional groups have been introduced into POCs to modulate the chemical environment for CO_2/CH_4 separations.[26] This concept was also recently translated to the liquid state in Type II porous liquids with POCs that dissolve in bulky organic solvents.[18] Here, we sought to transfer this concept to Type III porous liquids by using quasiracemic cocrystals.

Two systems were studied: **CC3**-*R/***CC15**-*S* and **CC3**-*R/***CC19**-*S* (Figure 2a). **CC15** is isostructural with **CC3**, but methyl groups occupy the four windows and reduce the window size to 1.7 Å (from 4 Å in **CC3**).[18] The reduced cage window size in **CC15** affects gas sorption in the internal cavities and in the portal sites, with the methyl groups both excluding larger guests and interfering with electrostatic interactions of guest molecules with the imine bonds. For example, CO_2 and Xe uptakes in **CC15** were approximately half as large as for **CC3** in the solid state,[12] and this occlusion was even more pronounced in a **CC15**-derived Type II porous liquid, where the Xe uptake was almost shut off entirely.[18] **CC19** has an analogous molecular structure, but with one hydroxyl group attached to each of its four aromatic rings. The incorporation of these polar hydroxyl groups improves the CO_2 uptake in the solid state compared to **CC3**, while lowering CH_4 uptakes.[26] Hence, by incorporating either **CC15** or **CC19** into the microparticles, there is an opportunity to tune the gas selectivity in the corresponding Type III porous liquids.

14

As might be expected, both the CO_2 and CH_4 uptakes in the 12.5 wt. % dispersion of **CC3**-*R*/**CC15**-*S* in silicone oil were significantly reduced compared to the **CC3**-*R/***CC3**-*S* liquid (CO_2: 68.5 ± 1.3 μmol/g_L vs 198.0 ± 3.8 μmol/g_L; CH_4: 30.2 ± 0.3 μmol/g_L vs 105.2 ± 16.5 μmol/g_L). By contrast, a slightly higher CO_2 uptake, and broadly comparable CH_4 uptake, were observed in the 12.5 wt. % dispersion of **CC3**-*R*/**CC19**-*S* in silicone oil (CO_2: 210.3 ± 3.3 μmol/g_L; CH_4: 117.4 ± 21.4 μmol/g_L) (Figure S26-S28). The reduction in porosity upon introducing **CC15**-*S* is likely due to the methyl groups blocking the cage windows. While incorporation of **CC19** into the microparticles improved gas uptakes in the Type III porous liquids, no significant enhancement in CO_2/CH_4 selectivity was observed, unlike in the solid state. This is probably due to its homogeneous distribution in the **CC3**-*R*/**CC19**-*S* microparticles, because previous studies[26] found that CO_2/CH_4 selectivity only occurred when **CC19** was included in a core-shell morphology. The use of such core-shell co-crystals to form selective Type III porous liquids is a subject for future studies.

Conclusions

We present here the first Type III porous liquids based on the dispersion of POC microparticles prepared by chiral recognition between chirally-opposed isostructural cages. A selection of size-excluded carrier liquids was investigated, including oils and ionic liquids, which can be used to tailor the porous liquids to meet application requirements. We were able to access liquids with relatively low viscosity, high thermal stability, or good recyclability, while maintaining properties such as gas solubility and colloidal stability. A 12.5 wt. % **CC3**-*R/***CC3**-*S* dispersion in silicone oil or [BPy][NTf_2] showed an approximate 2-fold increase in CO_2 uptake over the neat silicone oil, and up to 8 times the CH_4 uptake. These POC microparticle dispersions maintained their gas adsorption properties for at least one month and showed good colloidal stability. **CC3**-*R/***CC3**-*S* dispersions in [BPy][NTf_2] suffered no mass loss until 325 °C, and demonstrated a working capacity of 104.30 μmol/g_L by temperature swing (25–100 °C). These liquids were recyclable over at least ten CO_2 adsorption/desorption cycles. The incorporation of **CC15** into the microparticles reduced the CO_2 and CH_4 uptakes significantly, while inclusion of **CC19** increased the uptake of these gases, demonstrating the feasibility of fine-tuning gas sorption properties in Type III porous liquids by changing the microparticle components. Other potential applications for the future include the separation of volatile organic compounds or chiral separations using POC porous liquids.[36,37]

Acknowledgements

Author contributions

A.K., B.D.E., and R.L.G. carried out the cage synthesis, characterisation, thermal studies, and property investigation of the cage microparticles and Type III porous liquids. M.A.L. carried out the PXRD measurements on the cage microparticles and Type III porous liquids. A.I.C. and R.L.G. conceived the project, and the paper was written by A.K., B.D.E. and R.L.G. with input from all authors.

Corresponding authors

Correspondence to R. L. Greenaway or A. I. Cooper

Competing Interests

The authors declare no conflict of interest.

References

1   N. O'Reilly, N. Giri and S. L. James, *Chem. Eur. J.*, 2007, **13**, 3020–3025.

2   A. Bavykina, A. Cadiau and J. Gascon, *Coord. Chem. Rev.*, 2019, 386, 85–95.

3   J. Cahir, M. Y. Tsang, B. Lai, D. Hughes, M. A. Alam, J. Jacquemin, D. Rooney and S. L. James, *Chem. Sci.*, 2020, **11**, 2077–2084.

4   H. Li, B. Liu, M. Yang, D. Zhu, Z. Huang, W. Chen, L. Yang and G. Chen, *Ind. Eng. Chem. Res.*, 2020, **59**, 6154–6163.

5   W. Shan, P. F. Fulvio, L. Kong, J. A. Schott, C. L. Do-Thanh, T. Tian, X. Hu, S. M. Mahurin, H. Xing and S. Dai, *ACS Appl. Mater. Interfaces*, 2018, **10**, 32–36.

6   M. Costa Gomes, L. Pison, C. Červinka and A. Padua, *Angew. Chemie Int. Ed.*, 2018, **57**, 11909–11912.

7   S. Liu, J. Liu, X. Hou, T. Xu, J. Tong, J. Zhang, B. Ye and B. Liu, *Langmuir*, 2018, **34**, 3654–3660.

8   H. Liu, B. Liu, L. C. Lin, G. Chen, Y. Wu, J. Wang, X. Gao, Y. Lv, Y. Pan, X. Zhang, X. Zhang, L. Yang, C. Sun, B. Smit and W. Wang, *Nat. Commun.*, 2014, **5**, 5147–5153.

9   T. Tozawa, J. T. A. Jones, S. I. Swamy, S. Jiang, D. J. Adams, S. Shakespeare, R. Clowes, D. Bradshaw, T. Hasell, S. Y. Chong, C. Tang, S. Thompson, J. Parker, A. Trewin, J. Bacsa, A. M. Z. Slawin, A. Steiner and A. I. Cooper, *Nat. Mater.*, 2009, **8**, 973–978.

10   F. Beuerle and B. Gole, *Angew. Chemie Int. Ed.*, 2018, **57**, 4850–4878.

11   M. Mastalerz, *Acc. Chem. Res.*, 2018, **51**, 2411–2422.

12   A. G. Slater, P. S. Reiss, A. Pulido, M. A. Little, D. L. Holden, L. Chen, S. Y. Chong, B. M. Alston, R. Clowes, M. Haranczyk, M. E. Briggs, T. Hasell, G. M. Day and A. I. Cooper, *ACS Cent. Sci.*, 2017, **3**, 734–742.

13   N. Giri, M. G. Del Pópolo, G. Melaugh, R. L. Greenaway, K. Rätzke, T. Koschine, L. Pison, M. F. C. Gomes, A. I. Cooper and S. L. James, *Nature*, 2015, **527**, 216–220.

14   R. L. Greenaway, D. Holden, E. G. B. Eden, A. Stephenson, C. W. Yong, M. J. Bennison, T. Hasell, M. E. Briggs, S. L. James and A. I. Cooper, *Chem. Sci.*, 2017, **8**, 2640–2651.

15   R. J. Kearsey, B. M. Alston, M. E. Briggs, R. L. Greenaway and A. I. Cooper, *Chem. Sci.*, 2019, **10**, 9454–9465.

16   N. Giri, C. E. Davidson, G. Melaugh, M. G. Del Pópolo, J. T. A. Jones, T. Hasell, A. I. Cooper, P. N.

Horton, M. B. Hursthouse and S. L. James, *Chem. Sci.*, 2012, **3**, 2153–2157.

17   G. Melaugh, N. Giri, C. E. Davidson, S. L. James and M. G. Del Pópolo, *Phys. Chem. Chem. Phys.*, 2014, **16**, 9422–9431.

18   B. D. Egleston, K. V. Luzyanin, M. C. Brand, R. Clowes, M. E. Briggs, R. L. Greenaway and A. I. Cooper, *Angew. Chemie Int. Ed.*, 2020, **59**, 7362-7366.

19   T. Hasell, S. Y. Chong, K. E. Jelfs, D. J. Adams and A. I. Cooper, *J. Am. Chem. Soc.*, 2012, **134**, 588–598.

20   P. Li, H. Chen, J. A. Schott, B. Li, Y. Zheng, S. M. Mahurin, D. E. Jiang, G. Cui, X. Hu, Y. Wang, L. Li and S. Dai, *Nanoscale*, 2019, **11**, 1515–1519.

21   S. He, L. Chen, J. Cui, B. Yuan, H. Wang, F. Wang, Y. Yu, Y. Lee and T. Li, *J. Am. Chem. Soc.*, 2019, **141**, 19708–19714.

22   Y. Liu, Y. Bai and T. Tian, *Materials*, 2019, **12**, 3984–3991.

23   A. Knebel, A. Bavykina, S. J. Datta, L. Sundermann, L. Garzon-Tovar, Y. Lebedev, S. Durini, R. Ahmad, S. M. Kozlov, G. Shterk, M. Karunakaran, I. D. Carja, D. Simic, I. Weilert, M. Klüppel, U. Giese, L. Cavallo, M. Rueping, M. Eddaoudi, J. Caro and J. Gascon, *Nat. Mater.*, 2020, 1–8.

24   R. E. Mow, A. S. Lipton, S. Shulda, E. A. Gaulding, T. Gennett and W. A. Braunecker, *J. Mater. Chem. A*, 2020, **8**, 23455–23462.

25   J. Cravillon, S. Münzer, S. J. Lohmeier, A. Feldhoff, K. Huber and M. Wiebcke, *Chem. Mater.*, 2009, **21**, 1410–1412.

26   S. Jiang, Y. Du, M. Marcello, E. W. Corcoran, D. C. Calabro, S. Y. Chong, L. Chen, R. Clowes, T. Hasell and A. I. Cooper, *Angew. Chemie Int. Ed.*, 2018, **57**, 11228–11232.

27   J. T. A. Jones, T. Hasell, X. Wu, J. Bacsa, K. E. Jelfs, M. Schmidtmann, S. Y. Chong, D. J. Adams, A. Trewin, F. Schiffman, F. Cora, B. Slater, A. Steiner, G. M. Day and A. I. Cooper, *Nature*, 2011, **474**, 367–371.

28   T. Hasell, S. Y. Chong, M. Schmidtmann, D. J. Adams and A. I. Cooper, *Angew. Chemie Int. Ed.*, 2012, **51**, 7154–7157.

29   S. Tothadi, M. A. Little, T. Hasell, M. E. Briggs, S. Y. Chong, M. Liu and A. I. Cooper, *CrystEngComm*, 2017, **19**, 4933–4941.

30   M. Liu, L. Zhang, M. A. Little, V. Kapil, M. Ceriotti, S. Yang, L. Ding, D. L. Holden, R. Balderas-Xicohténcatl, D. He, R. Clowes, S. Y. Chong, G. Schütz, L. Chen, M. Hirscher and A. I. Cooper, *Science*, 2019, **366**, 613–620.

31   Silicone oil, Sigma-Aldrich, Gillingham, UK, MSDS - 317667,
        https://www.sigmaaldrich.com/MSDS/MSDS/DisplayMSDSPage.do?country=GB&language=en&pro
        ductNumber=317667&brand=ALDRICH&PageToGoToURL=https%3A%2F%2Fwww.sigmaaldrich.com
        %2Fcatalog%2Fproduct%2Faldrich%2F317667%3Flang%3Den, (accessed 25 June 2020).

32   M. A. A. Rocha and L. M. N. B. F. Santos, *Chem. Phys. Lett.*, 2013, **585**, 59–62.

33   D. Lerche, *J. Dispers. Sci. Technol.*, 2002, **23**, 699–709.

34   G. T. Hermanson, in *Bioconjugate Techniques*, Elsevier, 2013, 549–587.

35   F. Yu, Y. Chen, X. Liang, J. Xu, C. Lee, Q. Liang, P. Tao and T. Deng, *Prog. Nat. Sci. Mater. Int.*, 2017,
        27, 531–542.

36   A. Kewley, A. Stephenson, L. Chen, M. E. Briggs, T. Hasell and A. I. Cooper, *Chem. Mater.*, 2015, **27**,
        3207–3210.

37   L. Chen, P. S. Reiss, S. Y. Chong, D. Holden, K. E. Jelfs, T. Hasell, M. A. Little, A. Kewley, M. E. Briggs, A.
        Stephenson, K. M. Thomas, J. A. Armstrong, J. Bell, J. Busto, R. Noel, J. Liu, D. M. Strachan, P. K.
        Thallapally and A. I. Cooper, *Nat. Mater.*, 2014, **13**, 954–960.